



Swansea University
Prifysgol Abertawe



Cronfa - Swansea University Open Access Repository

This is an author produced version of a paper published in :

Scripta Materialia

Cronfa URL for this paper:

<http://cronfa.swan.ac.uk/Record/cronfa33919>

Paper:

Yusenko, K., Riva, S., Carvalho, P., Yusenko, M., Arnaboldi, S., Sukhikh, A., Hanfland, M. & Gromilov, S. (2017).

First hexagonal close packed high-entropy alloy with outstanding stability under extreme conditions and electrocatalytic activity for methanol oxidation. *Scripta Materialia*, 138, 22-27.

<http://dx.doi.org/10.1016/j.scriptamat.2017.05.022>

This article is brought to you by Swansea University. Any person downloading material is agreeing to abide by the terms of the repository licence. Authors are personally responsible for adhering to publisher restrictions or conditions. When uploading content they are required to comply with their publisher agreement and the SHERPA RoMEO database to judge whether or not it is copyright safe to add this version of the paper to this repository.

<http://www.swansea.ac.uk/iss/researchsupport/cronfa-support/>

First hexagonal close packed high-entropy alloy with outstanding stability under extreme conditions and electrocatalytic activity for methanol oxidation

Kirill V. Yusenko,^{*} [a,b] Sephira Riva,^[a] Patricia A. Carvalho,^[c,d] Maria V. Yusenko,^[e]

Serena Arnaboldi,^[f] Aleksandr S. Sukhikh,^[g,h] Michael Hanfland,^[i]

Sergey A. Gromilov^[g,h]

^aCollege of Engineering Swansea University Bay Campus SA1 8EN, UK

^bInstitute of Solid State Chemistry Pervomaiskaia str. 91, 620990 Ekaterinburg, Russia

^cSINTEF Materials and Chemistry PB 124 Blindern, NO-0314, Oslo, Norway

^dCEFEMA, Instituto Superior Tecnico Av. Rovisco Pais, Lisboa, Portugal

^eKönigsberger Str. 136 49157 Münster, Germany

^fDipartimento di Chimica Università degli Studi di Milano 20133 Milano, Italy

^gDepartment of Naturel Science Novosibirsk State University Pirogova str. 2, 630090 Novosibirsk, Russia

^hDepartment of Crystal Chemistry Nikolaev Institute of Inorganic Chemistry Lavrentiev ave. 3, 630090 Novosibirsk, Russia

ⁱDr. M. Hanfland ESRF-The European Synchrotron 71 Avenue des Martyrs, 38000, Grenoble, France

* Corresponding author: College of Engineering, Swansea University, Bay Campus, SA1 8EN, Wales, UK; e-mail: k.yusenko@swansea.ac.uk

Abstract. Multi-component alloys containing 5 and 6 platinum group metals have been prepared by thermal decomposition of single-source precursors. It is the first successful example of high-entropy alloy preparation not requiring direct melting at high temperature or mechanical alloying, and can be further extended to other multicomponent metallic systems. Our single-source precursor strategy for the

preparation of multicomponent alloys can be considered as a new approach in the design and optimization of refractory high-entropy alloys for a broad range of applications. Thermal decomposition occurs at low temperatures (below 800°C in H₂ flow). The resulting hexagonal Ir_{0.19}Os_{0.22}Re_{0.21}Rh_{0.20}Ru_{0.19} alloy is the first example of a single-phase hexagonal high-entropy alloy. Heat treatment does not result in any phase changes up to 1500 K, which is a record temperature stability for a single-phase high-entropy alloy. Room temperature hydrostatic compression up to 45 GPa also highlights the system's stability as a single phase, with a bulk modulus smaller than individual platinum group metals (except Rh). The prepared alloys show pronounced electrocatalytic activity in methanol oxidation, which opens a route for the use of high-entropy alloys as materials for sustainable energy conversion.

Keywords: high-entropy alloys; high-pressure; high-temperature; single-source precursors; methanol electro-catalytic oxidation

1. Introduction

Multicomponent alloys with principal element concentration between 5 and 35 at. % are often referred to as High-Entropy Alloys (HEAs) and are attractive as materials with promising high-temperature, mechanical and chemical stability. Their name emphasizes the role of entropy in favouring the formation of single-phase disordered alloys without precipitation of multiple ordered and partially disordered phases [1].

Since the single-phase disordered structures which are typical for HEAs are considered responsible for their outstanding properties, a detailed investigation of model single-phase alloys would give an understanding of the general trends in their formation and stability. However, the formation of inter-grain precipitates also plays an important role in their mechanical and chemical features. Truly single-phase HEAs are relatively

rare and the search for systems with high thermal stability is challenging due to the large number of experimental parameters to be taken into consideration [2]. Many single-phase HEAs prepared from the melt display a metastable nature and undergo phase separation during or after heating. The formation enthalpy of intermetallic compounds is often high and cannot be compensated by configuration entropy.

The most widely studied single-phase HEAs consist of low-density first-row transition metals (Al, Co, Cr, Fe, Ni) or of refractory elements (Mo, Nb, Ta, W, Zr). Up to now, it is mainly body-centred cubic (*bcc*) and face-centred cubic (*fcc*) HEAs that have been investigated. Recently, several experimental and theoretical works were performed to develop *hcp*-structured HEAs. In the *4f* transition metal alloy family, GdHoLaTbY, DyGdLuTbTm and DyGdLuTbY were found to contain a mixture of *hcp*-structured alloy and unknown admixture phases [4]; whereas AlLiMg_{0.5}ScTi_{1.5} was reported to be mainly *hcp* phase after heat treatment of mechanically-alloyed powders [5]. The melting of hexagonal metals leads only to three- or four-component *hcp*-structured alloys, which are normally in equilibrium with ordered phases or quasicrystals, as in AlCuMg_xMnZn [4,6]. These results mark the failure of the traditional melting route for the synthesis of single-phase *hcp*-structured HEAs and thermodynamic limitations in the relative stability of *hcp*-structured alloys, in comparison with intermetallic phases.

Heavy hexagonal close packed (*hcp*) metals (mainly Os, Re, Ru, and Zr) exhibit high hardness, as well as excellent mechanical and chemical stability. The design of *hcp*-structured HEAs based on these elements can open tantalizing possibilities for material development. As an example, the improvement of mechanical properties and oxidation

stability in rhenium alloys is known as the “*rhenium effect*” and plays an important role in refractory alloy design and development [3].

Platinum group (PGM) and refractory metals (*i.e.* rhenium) can therefore be considered ideal candidates for a new class of *hcp*-structured HEAs. Ir, Pd, Pt and Rh have *fcc* crystal structures, while Os, Ru and Re have *hcp* crystal structures in ambient conditions. All metals have high importance as construction materials for extreme conditions, and are active heterogeneous catalysts. However, due to their high melting points, PGM-based alloys are not easily accessible for development. They have barely been considered as principal elements for multicomponent alloys and HEAs. Pd, Rh and Ru were used as principal elements in seven multicomponent alloys, mainly as a family of 4-component *hcp*-structured MoPdRhRu alloys [2]; to the best of our knowledge, Ir, Os, Pt and Re have never been considered as principal elements in HEAs [2]. The latter elements are particularly promising candidates for single-phase HEA development, because they form continuous solid solutions in a broad range of compositions with each other, and display high catalytic activity and exceptional mechanical, chemical and thermal stability under extreme conditions.

The purpose of the presented study is the rational development of *hcp*-structured HEAs based on PGMs. A single-phase *hcp*-structured alloy has been successfully prepared by thermal decomposition of a single-source precursor. High-temperature, high-pressure stability and electrocatalytic activity for methanol oxidation in an acidic medium was experimentally proven by powder X-ray diffraction and cyclic voltammetry.

2. Experimental details

hcp-Ir_{0.19}Os_{0.22}Re_{0.21}Rh_{0.20}Ru_{0.19} and *fcc*-Ir_{0.26}Os_{0.05}Pt_{0.31}Rh_{0.23}Ru_{0.15} single-phase HEAs, as well as three two-phase samples (compositions can be found in Tables 1 and S1), were prepared by thermal decomposition of single-source precursors. The starting salts [Ir(NH₃)₅Cl]Cl₂, [Rh(NH₃)₅Cl]Cl₂, and [Ru(NH₃)₅Cl]Cl₂ were prepared according to published protocols [7-9] from soluble chlorides IrCl₄•*x*H₂O, RhCl₃•*x*H₂O and RuCl₃•*x*H₂O. (NH₄)₂[IrCl₆], (NH₄)₂[OsCl₆], (NH₄)₂[PtCl₆] and (NH₄)₂[ReCl₆] were obtained from Sigma Aldrich. Precursors were synthesised from water solutions according to the following procedure, where the amounts of [M(NH₃)₅Cl]Cl₂ and (NH₄)₂[MCl₆] were calculated according to the general equation listed below in the main text: a mixture of chloropentaammine salts was dissolved in hot water and a mixture of hexachlorometallates was also dissolved in hot water. 2-3 drops of concentrated HCl solution were added to suppress hydrolysis. The hot solutions were mixed with intensive stirring and cooled to room temperature. The brownish crystalline precipitates were filtered, washed with cold water and acetone, and dried in air. The compounds are air stable and did not need any protective atmosphere. Metallic alloys were prepared by thermal decomposition of single-source precursors in 5-vol.-%-H₂/95-vol.-%-N₂ stream (25-30 minutes at 1073 K with cooling to RT for 10-12 h).

Morphology and elemental composition were analysed using a Hitachi S-4800 Field Emission scanning-electron microscope equipped for energy dispersive X-ray spectroscopy (EDS). The average elemental composition was obtained from 20 individual points. High-resolution transmission electron microscopy was performed with a probe-corrected FEI Titan G2 60-300 transmission electron microscope equipped with a SuperX EDS Bruker spectrometer and operated at 300 eV. The observations

were performed by bright-field transmission electron microscopy (TEM), by high-resolution transmission electron microscopy (HRTEM) as well as by high-angle annular dark field (HAADF) scanning TEM (STEM) using a probe current of ~ 100 pA and convergence and collection semi-angles of 32 mrad and 76-200 mrad range, respectively, with resulting spatial resolution ~ 0.8 Å.

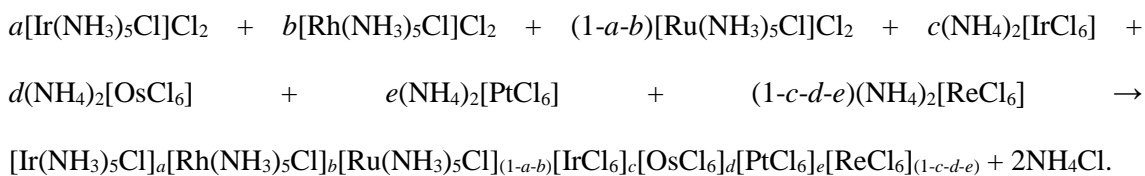
In situ high-temperature powder X-ray diffraction data were collected at the I11 beam-line at the DIAMOND light source ($\lambda = 0.494984$ Å). A wide-angle position sensitive detector based on Mythen-2 Si strip modules was applied to collect the diffraction data. The detector was moved at constant angular speed with 10 s scan time at each temperature, and 60 s waiting time in order to let the temperature stabilize. *hcp*- $\text{Ir}_{0.19}\text{Os}_{0.22}\text{Re}_{0.21}\text{Rh}_{0.20}\text{Ru}_{0.19}$ was sealed in 0.5 mm quartz capillary in vacuum, and heated in the capillary furnace from 25 to 1200 °C with axial rotation [10].

Room temperature compressibility curve was collected up to 45 GPa at the ID-15B beam-line, ESRF, ($\lambda = 0.410962$ Å, MAR 555 flat panel detector, beam size $10(v) \times 10(h)$ μm^2). The diffraction images were recorded under continuous ω -rotation of the DAC from -3 to $+3^\circ$ with an acquisition time of 1 second. The sample was loaded in a diamond anvil cell equipped with conically supported Boehler Almax type diamond anvils (300 μm culet sizes) [11]. The pressure was determined using a ruby placed in the pressure chamber and solid Ne as internal standard. Neon, serving as a pressure-transmitting medium, was loaded at about 1.5 kbar using the gas-loading system installed at the ID-15B beam-line. High-temperature and high-pressure radial diffraction data were calibrated, corrected and integrated using of the FIT2D [12] and refined using TOPAS [13]. Si (NIST SRM 640c) was used as an external standard for calibration.

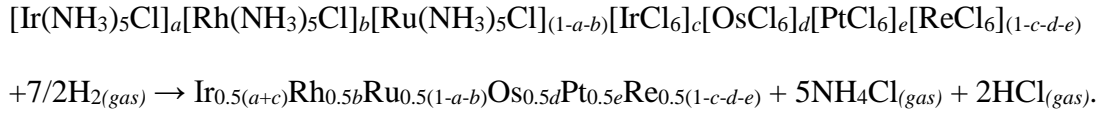
Cyclic voltammetry was performed using an Autolab PGSTAT potentiostat (Eco-Chemie) controlled by a PC with GPES software from the same manufacturer. Background measurements were performed in a drop of 1 M H₂SO₄. A few milligrams of powder were dispensed on screen-printed glassy carbon electrodes (GC-SPEs, DropSens C110, $S = 0.12 \text{ cm}^2$). Electro-catalytic tests were performed in a drop of 1 M MeOH / 1 M H₂SO₄ after 5 minutes of conditioning at 0.55 V (vs. SHE).

3. Results and discussion.

Our single-source strategy is based on the fact that isoformular solid crystalline salts containing coordination cations and coordination anions are usually isostructural, and can be co-crystallized with the formation of multicomponent salt solid solutions. Their thermal decomposition in a hydrogen stream or in an inert atmosphere results in the formation of multicomponent metallic alloys under relatively mild conditions (below 700-800 °C). For example, the reaction of water solutions of [Ir(NH₃)₅Cl]Cl₂ and (NH₄)₂[OsCl₆] results in precipitation of [Ir(NH₃)₅Cl][OsCl₆] [20-22]. [Ir(NH₃)₅Cl][OsCl₆] salt, which has low solubility in water and can be easily filtered. Further thermal decomposition below 800 °C in a hydrogen stream results in the formation of the metastable nanostructured *hcp*-Ir_{0.50}Os_{0.50} alloy. Similar reactions can be performed with other cations and anions including [Ru(NH₃)₅Cl]²⁺, [Rh(NH₃)₅Cl]²⁺, [IrCl₆]²⁻, [PtCl₆]²⁻, and [ReCl₆]²⁻ to co-crystallize 5- and 6-component salts:



Thermal decomposition in a hydrogen flow follows the general scheme, forming a multicomponent alloy:



Based on the co-crystallization of insoluble salts, several 5- and 6-component salts were prepared as single-source precursors for PGM-based HEAs (Table S1). All metals are equally distributed along the precursor, which ensures a higher probability of forming homogeneous multicomponent alloys, and suppressing aggregation and clustering of the resulting metallic phase. All solid individual precursors were decomposed in the reducing flow at 1073 K with the formation of *hcp*- and *fcc* single-phase metallic powders and *fcc+hcp* two-phase samples (Table 1).

Phase diagrams for multicomponent PGM-based alloy systems are not described in the literature [23]. However, several binary and ternary systems have been completely or partially investigated experimentally. The 6 metals (Pt, Ir, Rh, Ru, Os and Re) have 15 binary phase diagrams, including 3 *fcc-fcc* and 3 *hcp-hcp* binary phase diagrams with complete solubility in the solid state at high temperatures, as well as 9 *fcc-hcp* peritectic diagrams with a miscibility gap between *fcc*- and *hcp* alloys.

Binary and ternary PGM-based phase diagrams do not show large deviations from ideal-solution alloys, which also suggest minor deviation from the ideal situation in multicomponent systems. A 6-component Ir–Os–Pt–Re–Rh–Ru system can be constructed from two ternary sub-systems Os–Re–Ru (an *all-hcp* ternary system) and Ir–Pt–Rh (an *all-fcc* ternary system) with complete solubility in the solid state. Multicomponent alloys in 5- or 6-component systems should have a miscibility gap in *solidus* between *fcc* and *hcp* alloys which is similar to binary and ternary systems between *fcc* and *hcp* metals.

5- and 6-component alloys can therefore be classified by their ratio between *fcc*-structured (Rh, Ir, Pt, Pd) and *hcp*-structured (Ru, Re, Os) metals (Tables 1 and S1). The *hcp*-Ir_{0.19}Os_{0.22}Re_{0.21}Rh_{0.20}Ru_{0.19} HEA has a simplified composition of *hcp*_{0.61}*fcc*_{0.39}. Our data for multicomponent alloys suggest the maximum solubility of *fcc* metals in *hcp* to be <40 at.%, and the solubility of *hcp* metals in *fcc* to be <20 at.% (Table 1). This can be used to predict the formation of single-phase compositions in PGM-based multicomponent *hcp*_{*x*}*fcc*_{1-*x*} alloys.

4- and 5-component systems based only on *fcc*-structured metals (Ir–Pd–Pt–Rh) might be multiphase at moderate temperatures, due to the presence of a miscibility gap in solid state below *ca.* 1000°C between two *fcc*-structured alloys (*fcc*¹+*fcc*²) in Ir–Pt, Ir–Pd, Ir–Rh and Pd–Rh binaries [23]. Miscibility gaps in binary sub-systems should result in the formation of multiphase areas in the *solidus* region of multicomponent systems. The addition of other *fcc*-structured metals such as Cu, Ag and Au might result in the formation of intermetallic ordered phases, as occurs in Au–Pd, Cu–Pt and Cu–Pd systems. The miscibility gap in *fcc*-based 4- and 5-component alloys makes such systems less promising as precursors for single-phase HEAs. Nevertheless, phase diagrams and phase relations in *fcc*-based systems should be proven experimentally.

In contrast, light *hcp*-structured multicomponent systems such as Co–Sc–Ti–Y–Zr, which have been proposed as potential candidates for single-phase *hcp*-structured HEAs [4], show preferable formation of a number of ordered phases (CoSc, Au₃Cu- and *B*₂-type intermetallics). In other words, the *hcp*-structured single-phase HEA Ir_{0.19}Os_{0.22}Re_{0.21}Rh_{0.20}Ru_{0.19}, and its many combinations, currently represent the only candidates to be the forefathers of a large new class of *hcp* refractory alloys.

The single-phase $\text{Ir}_{0.19}\text{Os}_{0.22}\text{Re}_{0.21}\text{Rh}_{0.20}\text{Ru}_{0.19}$ HEA adopts an *hcp* structure with $P6_3/mmc$, $a = 2,728(1)$, $c = 4,338(2)$ Å, $V/Z = 13,979(2)$ Å³, $d_x = 18,364(1)$ g/cm³ (room temperature cell parameters, Fig. S1). Atomic volumes taken additively, according to alloy composition, suggest $V/Z = 13,877$ Å³, which corresponds to a 1 % negative deviation from the linear dependence of the alloys' atomic volumes (*Zen's law*) [24].

It is well known that single-phase HEAs are quite rare and usually stable only in a limited temperature interval. For example, a well-documented reversible phase separation in the *bcc*- $\text{Al}_x\text{CoCrFeNi}$ HEA family occurs above *ca.* 600 °C [25]. In contrast, a PGM-based single-phase *hcp*- $\text{Ir}_{0.24}\text{Os}_{0.21}\text{Re}_{0.16}\text{Rh}_{0.18}\text{Ru}_{0.20}$ HEA was heated in vacuum up to 1500 K to determine its thermal stability by high-temperature powder X-ray diffraction (Fig. 1). The volumetric thermal expansion coefficient for *hcp*- $\text{Ir}_{0.19}\text{Os}_{0.22}\text{Re}_{0.21}\text{Rh}_{0.20}\text{Ru}_{0.19}$ was estimated as: $\alpha(T) = 1.98(5) \cdot 10^{-5} + 1.5(2) \cdot 10^{-9} \cdot T$, by fitting the corresponding dataset to $\frac{V(T)}{Z} = \frac{V(T_0)}{Z} \exp \left[\int_{T_0}^T \alpha(T) dT \right]$, where $V(T_0)/Z$ is the atomic volume at reference temperature (293 K), and with $Z = 2$ for the *hcp* alloy. The HEA shows regular thermal expansion as a single phase, without distortions or phase transformations, up to 1500 K. *hcp*- $\text{Ir}_{0.24}\text{Os}_{0.21}\text{Re}_{0.16}\text{Rh}_{0.18}\text{Ru}_{0.20}$ HEA has relatively high thermal expansion and a small α_1 parameter, which is typical for Os and Re (Table 2). The corresponding *c/a* ratio increases with temperature, which is characteristic for Os and Ru. In contrast, the *c/a* ratio for pure Re decreases with temperature, which is quite rare for *hcp*-structured metals.

A higher concentration of *fcc*-structured metals in the alloy results in the formation of two-phase mixtures. Nevertheless, an *hcp*_{0.20}*fcc*_{0.80} alloy has been prepared as a single-phase *fcc*-structured alloy. Single-phase $\text{Ir}_{0.26}\text{Os}_{0.05}\text{Pt}_{0.31}\text{Rh}_{0.23}\text{Ru}_{0.15}$ has *fcc* crystal structure with space group $Fm \bar{3} m$, $a = 3.838(1)$ Å, $V/Z = 14,134(2)$ Å³, $d_x =$

18,655(1) g/cm³ (room temperature cell parameters, Fig. S4). Atomic volumes taken additively according to alloy composition suggest $V/Z = 14,254 \text{ \AA}^3$, corresponding to a 1 % positive deviation from Zen's law.

The phase stabilities of pure PGMs and Re have been intensively investigated under high pressure up to 304 GPa for Pt, 50 GPa for Rh, 56 GPa for Ru, 77 GPa for Pd, 640 for Re and 750 GPa for Os [26-28]. All of these metals seem to be incompressible (Table 2). Only elemental Ir, investigated up to 65 GPa, shows a 14-layered *hcp*-based superstructure above 59 GPa [29]. The corresponding equations of state for all PGM and Re are known in detail, and the pure metals (except Ir) show no HP—HT transformations. Pure Os investigated up to 750 GPa shows anomalies in the cell parameter ratio at 150 GPa and 440 GPa, which has been attributed to the change of the Fermi surface for valence electrons [30]. This electronic topological transition is mainly characteristic for *hcp*-structured metals and can be detected as an anomaly in the *c/a* behaviour under pressure. Despite this, the same transition has been predicted to occur in pure Ir at the much lower pressure of 80 GPa.

Since their development, HEAs have barely been investigated under high pressure. A hydrostatic compression of *fcc*-CrMnFeCoNi HEA reveals its martensitic transformation to the *hcp* phase at 14 GPa, which suggests a structural instability in HEAs under high pressure even at room temperature [31].

To prove its stability under extreme conditions, we investigated *hcp*-Ir_{0.19}Os_{0.22}Re_{0.21}Rh_{0.20}Ru_{0.19} at room temperature under compression up to 45 GPa, using Ne as a pressure transmitting medium. Its compressibility curve can be fitted with the third-order Birch-Murnaghan equation of state:

$$P(V) = \frac{3B_0}{2} \left[\left(\frac{V_0}{V} \right)^{\frac{7}{3}} - \left(\frac{V_0}{V} \right)^{\frac{5}{3}} \right] \left[1 + \frac{3}{4} (B_0' - 4) \left[\left(\frac{V_0}{V} \right)^{\frac{2}{3}} - 1 \right] \right],$$

where V_0 is the atomic volume at ambient pressure, B_0 the bulk modulus, and B_0' the pressure derivative of the bulk modulus (Table 2, Fig. 1). The *hcp*- $\text{Ir}_{0.19}\text{Os}_{0.22}\text{Re}_{0.21}\text{Rh}_{0.20}\text{Ru}_{0.19}$ HEA has low bulk modulus in comparison with pure PGMs. Only Rh shows lower bulk modulus, which was only measured by ultrasound measurements and should be proven by compressibility in diamond anvils. This can be a result of the large differences in compressibility for Os and other metals. The c/a ratio for *hcp*-HEA increases with pressure without any anomaly, which suggests no electronic topological transition above 45 GPa.

Transmission electron microscopy revealed that thermal decomposition in a N_2/H_2 gas stream produced foam-like polycrystalline aggregates with shapes similar to the starting single-source precursors (Fig. 2 (a) and (b)). High density of structural defects such as stacking faults and intergrowth were expected due to the relatively low preparation temperature. Nevertheless, few twin domains and planar defects were observed in the *hcp*- $\text{Ir}_{0.19}\text{Os}_{0.22}\text{Re}_{0.21}\text{Rh}_{0.20}\text{Ru}_{0.19}$ HEA. On the other hand, nanometric porosity was detected both at *inter*-granular and *intra*-granular regions (arrows in Fig. 2 (c) and (d), respectively). According to EDS data, all elements are homogeneously distributed within the phase (Fig. S8).

The two-phase sample presented similar foam-like polycrystalline aggregates without clear phase separation, which would be expected from the PXRD data (Fig. 3 and Fig. S3). Each particle contains regions of *fcc*- and *hcp*-intergrowths and high density of planar defects (Fig. 3b). Such structure is also typical for nano-twinned *fcc*- and *hcp*-structured alloys, and plays an important role in their mechanical properties, especially mechanical deformation. In the two-phase sample with nominal composition $\text{Ir}_{0.18}\text{Os}_{0.18}\text{Pt}_{0.16}\text{Re}_{0.17}\text{Rh}_{0.16}\text{Ru}_{0.15}$, elements show detectable segregation; Ir, Re and Os

concentrate inside grains while the presence of Pt, Ru and Rh is enhanced at grain boundaries (Fig. 3c-e). Segregation can be associated with a mechanism of thermal decomposition where metals are individually reduced at various temperatures.

Recently, several ternary [32-35] and quaternary [36] alloys based on PGMs were proposed as heterogeneous substrates for electro-catalysis. Particular attention has been given to active PGM-based multicomponent catalysts for methanol electro-oxidation, including the CoPtRu, OsPtRu, IrOsPtRu, NiPtRuZr, and NiPtRhRu systems [37-39].

The investigation of the catalytic activity of HEAs is at a very early stage. In fact, only $\text{Ag}_{0.08}\text{Co}_{0.10}\text{Cu}_{0.10}\text{Fe}_{0.11}\text{Ni}_{0.11}\text{Pt}_{0.52}$, CoCuFeNiPt and CuIrOsRuPt HEAs have been probed for methanol electro-oxidation [40-43]. The AlCoCrTiZn alloy was successfully tested for the catalytic degradation of azo-dye solutions [44]. In all cases, HEAs were prepared by sputtering or ball milling, techniques which are notoriously difficult to scale up. All studies concluded by reporting the high electro-catalytic activity of HEAs compared to binary and ternary alloys.

In the current study, methanol electro-oxidation has been chosen as a model reaction. The electro-oxidation of methanol in acidic media can be briefly described as a two-step process including the absorption and dehydrogenation of the molecule on the metallic surface and the oxidation of the adsorbate to CO_2 . So far, the best activity in this process has been shown by Pt–Ru alloys; but investigations have also been performed for Pd–Pt–Rh, Ir–Pt and Os [45-47].

We recorded the cyclic voltammograms following the adsorption of methanol at 0.55 V *versus* a standard hydrogen electrode (SHE) on pure metals and HEAs prepared via a single-phase precursor route. All platinum-group metals catalyse methanol oxidation (Fig. S5 and S6). The *hcp*- $\text{Ir}_{0.19}\text{Os}_{0.22}\text{Re}_{0.21}\text{Rh}_{0.20}\text{Ru}_{0.19}$ HEA and the two-

phase $\text{Ir}_{0.18}\text{Os}_{0.18}\text{Pt}_{0.16}\text{Re}_{0.17}\text{Rh}_{0.16}\text{Ru}_{0.15}$ also show a significant catalytic effect in the anodic oxidation of methanol in a sulfuric acid solution (Fig. 4).

Enhancement of the kinetics of methanol electro-oxidation is a well-documented effect for PGM alloys acting on transition metals, but the reason is still unclear. Either the alloying metal modifies the electronic structure of platinum valence bonds, therefore weakening the CO_{ads} binding and allowing the adsorbate to be removed more easily; or platinum atoms are responsible for the adsorption of methanol molecules, and the transition metal provides surface oxides which can oxidize the adsorbate at lower potentials. The latter might entail that nanostructured alloys favour electro-oxidation, as shown by the oxidation potential of the two-phase $\text{Ir}_{0.18}\text{Os}_{0.18}\text{Pt}_{0.16}\text{Re}_{0.17}\text{Rh}_{0.16}\text{Ru}_{0.15}$ vs. the single-phase *hcp*- $\text{Ir}_{0.19}\text{Os}_{0.22}\text{Re}_{0.21}\text{Rh}_{0.20}\text{Ru}_{0.19}$ (Figure 5: $E_{\text{ox}}^{\text{two-phase HEA}} = 0.503 \text{ V}$, $E_{\text{ox}}^{\text{hcp-HEA}} = 0.505 \text{ V}$ vs. SHE).

4. Conclusions.

Our single-source precursor strategy can be further extended to a large number of systems, such as salts with $[\text{M}(\text{NH}_3)_5\text{Cl}]^{2+}$ ($M = \text{Co}, \text{Cr}, \text{Ir}, \text{Os}, \text{Rh}, \text{Ru}$) and hexahalogeno-metallates $[\text{M}\Gamma_6]^{2-}$ ($M = \text{Ir}, \text{Os}, \text{Pd}, \text{Pt}, \text{Re}, \text{Ti}, \text{V}, \text{Zr}; \Gamma = \text{F}, \text{Cl}, \text{Br}, \text{I}$). A similar approach can be used to prepare multicomponent metallic alloys using other cations and anions, which can form isoformular isostructural salts. The chemical nature and composition of the single-source precursor affect the decomposition temperature, and potentially control the phase composition and morphology of the metallic alloys. Since the precursors are stable salts obtained from water solutions, our approach can be easily scaled up and used as an environmentally friendly chemical route for the preparation of multi-component supported catalysts for fuel cells. The decomposition of

single-source precursors occurs at low temperatures in non-equilibrium conditions. In some cases it offers metallic alloys unavailable by direct melting [7].

The first *hcp*-structured PGM-based 5-component HEA shows extraordinary stability under extreme conditions. The alloy has higher thermal expansion and lower bulk modulus in comparison with individual PGMs, an unexpected result, which requires further investigation. The high electro-catalytic activity of the investigated HEA systems could be related to the electronic effects often associated with alloys, or to the synergic effect inherent to HEAs and often referred to as “*cocktail effect*”. So far, a deeper understanding of the catalytic activity of HEAs has been hindered by the sensitivity of the alloy to its production route. The synthetic pathway herein reported, on the other hand, leads to highly reproducible results.

In perspective, our approach can be extended to other multicomponent systems and further improve catalytic activity. The small amounts of powder used for each experiment suggest an application as a micro-preparative technique in new alloy screening, as well as a fast tool for phase diagram construction of multicomponent systems. Our high-entropy alloys prepared from single-source precursors can be used as prototypes for metallic foams due to a present of nano-pores.

Acknowledgements

The authors thank the I11 beam-line at the DIAMOND LS, the ID15B beam-line at ESRF, and NORTEM for providing us with measurement time and technical support. SR gratefully acknowledges the financial support provided by the Welsh Government and Higher Education Funding Council for Wales through the Sêr Cymru National Research Network in Advanced Engineering and Materials, and the Materials Advanced Characterisation Centre. KVV is grateful to the EPSRC Impact Acceleration Account.

References:

- [1] A.D. Pogrebnjak, A.A. Bagdasaryan, I.V. Yakushchenko, V.M. Beresnev, The structure and properties of high-entropy alloys and nitride coatings based on them, *Russ. Chem. Rev.* 83 (2014) 1027–1061, <https://doi.org/10.1070/RCR4407>
- [2] D.B. Miracle, O.N. Senkov, A critical review of high entropy alloys and related concepts, *Acta Mater.* 122 (2017) 448–511, <http://doi.org/10.1016/j.actamat.2016.08.081>
- [3] M. Huang, J. Zhu, *Rare Met.*, An overview of rhenium effect in single-crystal superalloys, 35 (2016) 127–139, DOI: 10.1007/s12598-015-0597-z
- [4] Y.L. Chen, C.W. Tsai, C.C. Juan, M.H. Chuang, J.W. Yeh, T.S. Chin, S.-K. Chen, Amorphization of equimolar alloys with *HCP* elements during mechanical alloying, *J. Alloys Compd.* 2010, 506, 210–215, <http://doi.org/10.1016/j.jallcom.2010.06.179>
- [5] K.M. Yusef, A.J. Zaddach, Ch. Niu, D.L. Irving, C.C. Koch, Novel low-density, high-hardness, high-entropy alloy with close-packed single-phase nanocrystalline structures, *Mater. Res. Lett.*, 3 (2015) 95–99, <http://dx.doi.org/10.1080/21663831.2014.985855>
- [6] R. Li, J. Gao, K. Fan, Study to Microstructure and Mechanical Properties of Mg Containing High Entropy Alloys, *Mater. Sci. Forum*, 650 (2010) 265–271, DOI 10.4028/www.scientific.net/MSF.650.265
- [7] S.V. Korenev, A.B. Venediktov, K.V. Yusenkov, Yu.V. Shubin, Synthesis and properties of $[\text{Rh}(\text{NH}_3)_5\text{Cl}][\text{PtCl}_4]$, *Russ. J. Coord. Chem.*, 26 (2000) 358–360.

- [8] Yu.V. Shubin, S.V. Korenev, K.V. Yusenko, T.M. Korda, A.B. Venediktov, X-ray study of double complex salts $[M(NH_3)_5Cl][M^*Cl_4]$ – precursors of polymetallic powders (where $M = Ir, Rh, Co$; $M^* = Pt, Pt$), *Russ. Chem. Bull.*, 51 (2002) 39–43.
- [9] S.A. Martynova, K.V. Yusenko, I.V. Korolkov, S.A. Gromilov, Synthesis, properties, and thermal decomposition products of $[Ru(NH_3)_5Cl][PtCl_6]$ and $[Ru(NH_3)_5Cl]_2[PtCl_6]Cl_2$, *Russ. J. Coord. Chem.*, 33 (2007) 530–534.
- [10] S.P. Thompson, J.E. Parker, J. Marchal, J. Potter, A. Birt, F. Yuang, R.D. Fearn, A.R. Lennie, S.R. Street, C.C. Tang, Fast X-ray powder diffraction on I11 at Diamond, *J. Synchrotron Rad.*, 18 (2011) 637–648, DOI: 10.1107/S0909049511013641.
- [11] R. Boeler, K. De Hantsetters, New anvil designs in diamond-cells, *High Pressure Research*, 24 (2004) 391–396, <http://dx.doi.org/10.1080/08957950412331323924>.
- [12] A.P. Hammersley, S.O. Svensson, M. Hanfland, A.N. Fitch, D. Häusermann, Two-dimensional detector software: From real detector to idealised image or two-theta scan, *High Press. Res.*, 14 (1996) 235–248, <http://dx.doi.org/10.1080/08957959608201408>.
- [13] TOPAS v.4.0, Bruker-AXS 5465 East Cheryl Parkway – Bruker AXS – 2009.
- [14] J.W. Arblaster, Crystallographic Properties of Platinum, *Platinum Met. Rev.*, 41 (1997) 12–21
- [15] J.W. Arblaster, Crystallographic Properties of Rhodium, *Platinum Met. Rev.*, 41 (1997) 184–189.
- [16] J.W. Arblaster, Crystallographic Properties of Iridium, *Platinum Met. Rev.*, 54 (2010) 93–102, doi:10.1595/147106710x493124
- [17] J.W. Arblaster, Crystallographic Properties of Osmium, *Platinum Met. Rev.*, 57 (2013) 177–185, doi:10.1595/147106713x668541

- [18] J.W. Arblaster, Crystallographic Properties of Ruthenium, *Platinum Met. Rev.*, 57 (2013) 127–136, doi:10.1595/147106713x665030
- [19] V.G. Sovetnikova, V.V. Zubenko, M.M. Umansky, X-ray diffraction determination of thermal expansion of rhenium in a wide temperature range, *Kristallografiya (in Russian)*, 2(5) (1977), 1026–1029.
- [20] S.A. Gromilov, S.V. Korenev, I.A. Baidina, I.V. Korolkov, K.V. Yusenko, Syntheses of $[\text{Rh}(\text{NH}_3)_5\text{Cl}][\text{MCl}_6]$ ($\text{M} = \text{Re}, \text{Os}, \text{Ir}$) and investigation of their thermolysis products. Crystal structure of $[\text{Rh}(\text{NH}_3)_5\text{Cl}][\text{OsCl}_6]$, *J. Struct. Chem.*, 43 (2002) 488–494.
- [21] S.V. Korenev, A.B. Venediktov, Yu.V. Shubin, S.A. Gromilov, K.V. Yusenko, Synthesis and structure of binary complexes of platinum group metals — precursors of metallic materials, *J. Struct. Chem.*, 44 (2003) 46–59.
- [22] I.V. Korolkov, S.A. Gromilov, K.V. Yusenko, I.A. Baidina, S.V. Korenev, Crystal structure of the $[\text{Ir}(\text{NH}_3)_5\text{Cl}]_2[\text{OsCl}_6]\text{Cl}_2$. Crystal analysis of the Ir—Os metallic system, *J. Struct. Chem.*, 46 (2005) 1052–1059.
- [23] H. Chunxiao, Li Guanfang, *Phase diagrams of Precious Metal Alloys and Structure Parameters of Precious Metal Compounds*, Met. Press., Beijing 2010, 724 p.
- [24] Zen. E-an, Validity of “Vegard’s Law”, *Am. Mineral.* 41 (1956) 523–524.
- [25] L.J. Santodonato, Y. Zhang, M. Feygenson, C.M. Parish, M.C. Gao, R.J.K. Weber, J.C. Neufeind, Z. Tang, P.K. Liaw, Deviation from high-entropy configurations in the atomic distributions of a multi-principal-element alloy, *Nature Commun.*, 6 (2015) 5964, doi: 10.1038/ncomms6964
- [26] Tonkov and Ponyatovsky (2005): *Phase transformations of elements under high pressure*, CRC Press LLC, 377 p.

- [27] L. Dubrovinsky, N. Dubrovinskaia, V. Prakapenka, A. Abakumov, Implementation of micro-ball nanodiamond anvils for high-pressure studies above 6 Mbar, *Nature Commun.*, 3 (2012) 1163, DOI: 10.1038/ncomms2160
- [28] L. Dubrovinsky, N. Dubrovinskaia, E. Bykova, M. Bykov, V. Prakapenka, C. Prescher, H.-P. Liermann, M. Hanfland, M. Ekholm, Q. Feng, L.V. Pourovskii, M.I. Katsnelson, J.M. Wills, I.A. Abrikosov, The most incompressible metal osmium at static pressures above 750 gigapascals, *Nature*, 525 (2015) 226–229, DOI: 10.1038/nature14681
- [29] Y. Cerenius, L. Dubrovinsky, Compressibility measurements on iridium, *J. Alloys Comp.* 306 (2000) 26–29, [http://dx.doi.org/10.1016/S0925-8388\(00\)00767-2](http://dx.doi.org/10.1016/S0925-8388(00)00767-2)
- [30] A.A. Tal, M.I. Katsnelson, M. Ekholm, H.J.M. Jönsson, L. Dubrovinsky, N. Dubrovinskaia, I.A. Abrikosov, Pressure-induced crossing of the core levels in 5d metals, *Phys. Rev. B*, 93 (2016) 205150, <https://doi.org/10.1103/PhysRevB.93.205150>
- [31] C.L. Tracy, S. Park, D.R. Rittman, S.J. Zinkle, H. Bei, M. Lang, R.C. Ewing, W.L. Mao, <https://arxiv.org/abs/1611.00876>
- [32] R. Srivastava, P. Mani, N. Hahn, P. Strasser, Efficient oxygen reduction fuel cell electrocatalysis on voltammetrically dealloyed Pt–Cu–Co nanoparticles, *Angew. Chem. Int. Ed.*, 47 (2007) 8988–8991, DOI: 10.1002/anie.200703331.
- [33] Z.-L. Wang, J.-M. Yan, Y. Ping, H.-L. Wang, W.-T. Zheng, Q. Jiang, An Efficient CoAuPd/C Catalyst for Hydrogen Generation from Formic Acid at Room Temperature, *Angew. Chem. Int. Ed.*, 52 (2013) 4406–4409, DOI: 10.1002/ange.201301009.

- [34] Q. Li, X. Wen, G. Wu, H.T. Chung, R. Gao, P. Zelenay, High-activity PtRuPd/C catalyst for direct dimethyl ether fuel cells, *Angew. Chem. Int. Ed.*, 54 (2015) 7524–7528, DOI:10.1002/anie.201500454
- [35] J.W. Hong, Y. Kim, D.H. Wi, S. Lee, S.-U. Lee, Y.W. Lee, S.-I. Choi, S.W. Han, Ultrathin Free-Standing Ternary-Alloy Nanosheets, *Angew. Chem. Int. Ed.*, 55 (2016) 2753–2758, DOI: 10.1002/anie.201510460
- [36] L. Liu, E. Pippel, Low-Platinum-Content Quaternary PtCuCoNi Nanotubes with Markedly Enhanced Oxygen Reduction Activity, *Angew. Chem. Int. Ed.*, 50 (2011) 2729–2733, DOI: 10.1002/anie.201006644
- [37] B. Gurau, R. Viswanathan, R. Liu, T. J. Lafrenz, K. L. Ley, E. S. Smotkin, E. Reddington, A. Sapienza, B. C. Chan, T. E. Mallouk, S. Sarangapani, Structural and Electrochemical Characterization of Binary, Ternary, and Quaternary Platinum Alloy Catalysts for Methanol Electro-oxidation, *J. Phys. Chem. B*, 102 (1998) 9997, DOI: 10.1021/jp982887f
- [38] E. Reddington, A. Sapienza, B. Gurau, R. Viswanathan, S. Sarangapani, E. S. Smotkin, T. Mallouk, Combinatorial Electrochemistry: A Highly Parallel, Optical Screening Method for Discovery of Better Electrocatalysts, *Science*, 280 (1998) 1735–1737, DOI: 10.1126/science.280.5370.1735
- [39] P. Strasser, Q. Fan, M. Devenney, W. H. Weinberg, P. Liu, J. K. Nørskov, High Throughput Experimental and Theoretical Predictive Screening of Materials – A Comparative Study of Search Strategies for New Fuel Cell Anode Catalysts, *J. Phys. Chem. B* 2003, 107, 11013, DOI: 10.1021/jp030508z

- [40] C.-F. Tsai, P.-W. Wu, P. Lin, C.-G. Chao, K.-Y. Yeh, Sputter Deposition of Multi-Element Nanoparticles as Electrocatalysts for Methanol Oxidation, *Jap. J. Appl. Phys.*, 47 (2008) 5755–5761, <https://doi.org/10.1143/JJAP.47.5755>
- [41] C.-F. Tsai, K.Y. Ye, P.-W. Wu, Y.-F. Hsieh, P. Lin, Effect of platinum present in multi-element nanoparticles on methanol oxidation, *J. Alloys Compd.*, 478 (2009) 868–871, <http://doi.org/10.1016/j.jallcom.2008.12.055>
- [42] A.-L. Wang, H.-C. Wan, H. Xu, Y.-X. Tong, G.-R. Li, Quinary PdNiCoCuFe Alloy Nanotube Arrays as Efficient Electrocatalysts for Methanol Oxidation, *Electrochim. Acta*, 127 (2014) 448–453, <http://doi.org/10.1016/j.electacta.2014.02.076>
- [43] X. Chen, C. Si, Y. Gao, J. Frenzel, J. Sun, G. Eggeler, Z. Zhang, Multi-component nanoporous platinum–ruthenium–copper–osmium–iridium alloy with enhanced electrocatalytic activity towards methanol oxidation and oxygen reduction, *J. Power Sources*, 273 (2015) 324–332, <http://doi.org/10.1016/j.jpowsour.2014.09.076>
- [44] Z.Y. Lv, X.J. Liu, B. Jia, H. Wang, Y. Wu, Z.P. Lu, Development of a novel high-entropy alloy with eminent efficiency of degrading azo dye solutions, *Scientific Rep.*, 6 (2016) 34213, DOI: 10.1038/srep34213
- [45] A. Aramata, T. Yamazaki, K. Kunimatsu, M. Enyo, Electrooxidation of methanol on iridium in acidic solutions: electrocatalysis and surface characterization by infrared spectroscopy, *J. Phys. Chem.*, 91 (1987) 2309–2314, DOI: 10.1021/j100293a020
- [46] G. Orozco, C. Gutiérrez, Adsorption and electro-oxidation of carbon monoxide, methanol, ethanol and formic acid on osmium electrodeposited on glassy carbon, *J. Electroanal. Chem.*, 484 (2000) 64–72, [http://doi.org/10.1016/S0022-0728\(00\)00062-0](http://doi.org/10.1016/S0022-0728(00)00062-0)

[47] M.S. Ureta-Zanartu, P. Bravo, J.H. Zagal, Methanol oxidation on modified iridium electrodes, *J. Electroanal. Chem.*, 337 (1992) 241–251, [https://doi.org/10.1016/0022-0728\(92\)80541-B](https://doi.org/10.1016/0022-0728(92)80541-B)

Figure 1. Thermal expansion curves for *hcp*-Ir_{0.19}Os_{0.22}Re_{0.21}Rh_{0.20}Ru_{0.19} (*hcp*-HEA), pure PGMs [14-18] and rhenium [19] (*left*); temperature dependence of *c/a* ratio (*middle*); room temperature compressibility curve for *hcp*-Ir_{0.19}Os_{0.22}Re_{0.21}Rh_{0.20}Ru_{0.19} HEA in comparison with PGMs (*orange* – Os, *blue* – Ir, *green* – Re, *red* – Ru, *grey line* – Rh; insert shows *c/a* pressure dependence) (*right*).

Figure 2. (a) STEM HAADF image of metallic polycrystalline particles in single-phase *hcp*-Ir_{0.19}Os_{0.22}Re_{0.21}Rh_{0.20}Ru_{0.19} HEA. (b) Magnified detail of (a). (c) TEM image of a similar region. (c) High resolution HAADF images of grain boundaries. Pores at grain boundaries (c) and in grains (d) are indicated by arrows.

Figure 3. (a) TEM image of polycrystalline particle in two-phase HEA with nominal composition Ir_{0.18}Os_{0.18}Pt_{0.16}Re_{0.17}Rh_{0.16}Ru_{0.15}. (b) HRTEM image of squared detail in (a). (c) STEM HAADF image where the star and dashed line represent the same regions as in (b)). Pores are indicated by arrows. (d) Composition profile along the dashed line across a grain boundary. (e) Elemental distribution of Pt and Os in region (c).

Figure 4. Cyclic voltammograms (scan rate 0.1 V s⁻¹) recorded in 1 M MeOH / 1 M H₂SO₄ after 5 min of methanol absorption at 0.55 V on (a) single-phase *hcp*-Ir_{0.19}Os_{0.22}Re_{0.21}Rh_{0.20}Ru_{0.19} HEAs.; (b) two-phase Ir_{0.18}Os_{0.18}Pt_{0.16}Re_{0.17}Rh_{0.16}Ru_{0.15}. *Blue line* – first cycle after absorption; *grey line* – second cycle after absorption (background). Current is normalised for the working electrode surface area. Potentials are reported against the standard hydrogen electrode (SHE) by using the ferrocyanide | ferricyanide redox couple as an internal standard.